JOM, Vol. 75, No. 2, 2023
https://doi.org/10.1007/s11837-022-05507-6

Recovery of Lithium from Spent Coin-Type Lithium Manganese Dioxide CR Cells by Acidic Leaching in the Presence of Potassium Permanganate as Oxidant

SAIT KURSUNOGLU ,[1,6] SONER TOP,[2] MAHMUT ALTINER,[3] SAFAK OZSARAC,[4] and MUAMMER KAYA[5]

1.—Department of Petroleum and Natural Gas Engineering, Batman University, 72100 Batman, Turkey. 2.—Department of Nanotechnology Engineering, Abdullah Gul University, 38100 Kayseri, Turkey. 3.—Department of Mining Engineering, Division of Mineral Processing, Cukurova University, 01330 Adana, Turkey. 4.—Department of Geological Engineering, Batman University, 72100 Batman, Turkey. 5.—Department of Mining Engineering, Division of Mineral Processing, Eskisehir Osmangazi University, 26480 Eskisehir, Turkey. 6.—e-mail: sait.kursunoglu@batman.edu.tr

The selective leaching of lithium from spent coin-type lithium manganese dioxide CR cells by oxidative leaching and precipitation of Li_2CO_3 from Li-bearing leach solution has been experimentally and theoretically investigated. The oxidative leaching experiments were carried out using sulfuric acid in the presence of potassium permanganate ($KMnO_4$). The dissolutions of lithium, manganese, nickel, and cobalt were found to be 84.8%, 0.9%, 46.6%, and 9.7%, respectively. The results demonstrated that a considerable amount of manganese and cobalt remained in the leach residue. The Li-bearing leach solution was fed to an impurity removal stage. It was observed that a substantial amount of lithium loss, along with manganese, nickel, and cobalt, was determined at pH 10. At standard temperature and pressure, the species of lithium as a function of pH, lithium concentration, and carbonate concentration was evaluated for the generation of Li_2CO_3 from the oxidative leach solution. The results revealed that the precipitation of lithium as lithium carbonate is thermodynamically feasible from the solution at high pHs.

INTRODUCTION

Lithium is a critical element of modern energy systems, and has attracted an increasing amount of scientific attention. It is added to glasses and ceramics, and serves as an alloying agent in the synthesis of organic compounds.[1] High-power lithium batteries are dedicated to aerospace and military applications and to electric vehicles, while coin-type lithium manganese dioxide batteries (CR-type batteries) are widely used in portable electronic devices, such as watches, calculators, cameras, computers, radios, sensors, and transmitters, as well as medicinal applications.[2–4] The batteries are composed of metallic lithium as the anode and manganese oxide as the cathode, lithium salts ($LiAsF_6$, $LiClO_4$, $LiPF_6$, $LiBF_4$) as electrolytes, propylene carbonate-dimethoxyethane and 1, 3-dioxolane as organic solvents, and polypropylene as a separator.[2,5] Not only primary but also secondary lithium batteries exhibit complementary electrochemical properties, and their use has significantly expanded in recent years, reaching up to 10,000 t/year.[5–7] CR batteries consist of 1.5–6% Li, 9.5–16% Mn, 34–42% Fe, 10% Cr, 3–6% Ni, and 0.1–1% Mo for a coin cell of an average weight of 3 g.[8,9] The batteries are typically discarded as household waste due to a lack of awareness, but they are classified as hazardous, toxic, and flammable waste materials that can cause major environmental problems.[4,6,10,11] Thus, it is essential to recycle depleted lithium manganese dioxide batteries in the scope of environmental responsibility,

(Received July 1, 2022; accepted August 29, 2022; published online September 20, 2022)

secondary resource conservation, and economic recovery of valuable metals, such as lithium and manganese.[5,12]

Numerous combinations of hydro- and pyro-metallurgical routes had been tested to produce electrolytic MnO_2 from pyrolusite and Mn-Fe ores and from spent alkaline batteries via pyrometallurgical reduction to MnO, using coal, hydrogen, and natural gas, followed by inorganic acid leaching or magnetic separation, purification, neutralization with lime, and electrolysis.[2,4,6,10,13–25] As green and efficient reagents, organic acids, such as oxalic and citric acid, have been widely used in hydrometallurgical processes for effective manganese recovery from manganese ore, in order to overcome the drawbacks of conventional pyrometallurgical methods.[26] However, these organic acids have resulted in low metal recovery.[13,27]

Recently, lithium-ion batteries (LIBs) have attracted attention for the recovery of valuable metals by selective leaching,[28–30] selective precipitation,[31–34] and solvent extraction.[35,36] By using selective leaching and precipitation, no desirable metal ion separation has been accomplished. Additionally, insufficient product purity has been reached at the cost of considerable reagent usage, difficult processes, and solid entrainment.[37] However, organic acids, like oxalic acid[38] and tartaric acid,[39] have exhibited high selectivity for Li over other metals during the leaching of waste LIBs. The solvent extraction process has also demonstrated excellent separation efficiency, which enables the final product to match the needed fields' requirements. Numerous studies on the co-extraction of Ni-Co-Mn from pregnant leach solutions have been conducted by D2EHPA. For example, whereas Ni-Co-Mn has been taken almost completely into the organic phase, only 30% of Li has been extracted.[40] Although the extractant Versatic 10 is capable of separating the transition metal from lithium, it requires additional extraction stages and alkali solutions to neutralize the leachate in order to achieve high pHs.[41] The extractant P227 has also been used to separate heavy rare earth metals and cathode materials due to its extraordinary chemical properties, such as excellent separation ability and saturation capacity.[42–44] Sulfidation–roasting–leaching for the recovery of Li from LIBs has been proposed as a novel technology, based on the use of acidic sulfates ($(NH_4)_2SO_4$, $NaHSO_4$, and $MgSO_4$) to convert active materials ($LiCoO_2$) into soluble Li_2SO_4 and insoluble Co_3O_4 via roasting at temperatures ranging from 600 to 800 °C. As a result, this roast product has been processed with water leaching to produce a Li-rich sulfate solution from which pure Li_2CO_3 precipitates.[45]

Although recent studies have concentrated on metal extraction from spent lithium-ion, alkaline, and nickel-metal hydrate batteries, no study has been conducted to extract lithium from spent coin-type lithium manganese dioxide CR cells via oxidative leaching. Therefore, this study has investigated the selective leaching of lithium from spent coin-type CR cells' black paste using potassium permanganate as a strong oxidant in sulfuric acid solution, leaving a bulky amount of manganese in the leach residue. In addition, the thermodynamic possibility of an Li-rich leach solution precipitation with Na_2CO_3 to obtain a high purity of Li_2CO_3 final product has been theoretically demonstrated.

MATERIALS AND METHODS

Materials

Spent coin-type lithium manganese dioxide CR cells were generously provided by an Ankara-based battery collector. Prior to conducting the oxidative leaching experiments, the cells were crushed to dismantle the steel casings, using a laboratory-type jaw crusher. The crushed materials were then manually sieved through a 1-mm sieve to remove unnecessary items, such as steel casings, separators, plastics, and grids from the black paste containing lithium manganese dioxide. The generated black paste was dried in a 60 °C oven until the sample reached a constant weight. The dried material was ground manually in a mortar to a particle size of less than 212 μm. The materials were homogenized and used in all stages of the study. The spent, crushed coin cells and ground material are shown in Fig. 1. X-ray fluorescence (XRF; Panalytical MiniPal 4), inductively-coupled plasma (ICP-MS; Perkin Elmer), and atomic absorption spectrometry (AAS; PinAAcle 900F; Perkin Elmer) analyses were carried out to assess the chemical composition of the material. To evaluate the sample's mineralogical components, x-ray diffraction (XRD) analysis was performed using a Bruker D8 Discover system fitted with a Lynxeye detector. The XRD data were collected over a 15-min period with a 0.02° step size in the 10°–90° range. The Diffrac.-Suite Eva software with an up-to-date PDF 2 database was used to identify the minerals. The surface morphology of the lithium manganese dioxide black paste and the oxidative leach residue were determined by field-emission scanning electron microscopy (SEM).

Methods

Prior to conducting the oxidative leaching experiments, preliminary leaching tests were carried out in sulfuric acid (H_2SO_4; Merck, Belgium) solution according to the Taguchi approach (Table I), which leads to the obtaining of satisfactory results from a minimum number of experiments. The effects of sulfuric acid concentration, leaching time, and leaching temperature on the lithium, manganese, nickel, and cobalt dissolutions were determined. The selective dissolution of lithium from the investigated sample was examined using potassium permanganate ($KMnO_4$; Detsan, Turkey) as a

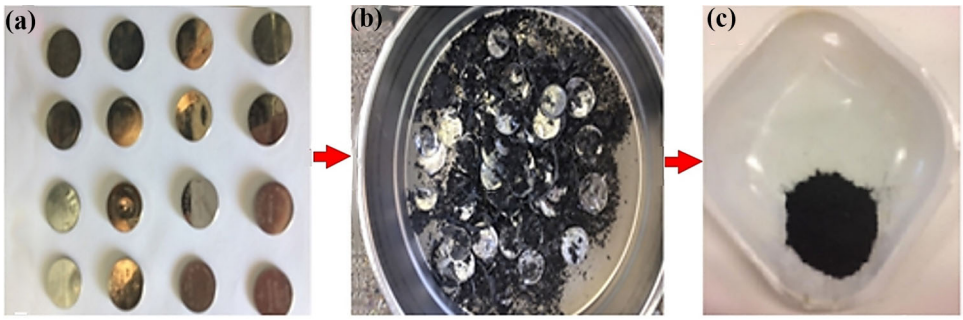

Fig. 1. Dismantling process: (a) spent coin cells, (b) crushed cells, (c) ground material.

Table I. Experimental parameters with their levels and conditions according to the Taguchi approach [L9 (3^3)]

Parameters	Symbol	Level 1	Level 2	Level 3
Acid concentration (mol/L)	1	0.5	1.25	2
Time (min)	2	60	90	120
Temperature (°C)	3	30	60	90

Exp. No	Acid concentration (mol/L)	Time (min.)	Temperature (°C)
E1	0.5	60	30
E2	0.5	90	60
E3	0.5	120	90
E4	1.25	60	60
E5	1.25	90	90
E6	1.25	120	30
E7	2	60	90
E8	2	90	30
E9	2	120	60

strong oxidant in sulfuric acid solution, leaving bulky manganese in the leach residue. The oxidative leaching tests were carried out in a 100-mL Erlenmeyer flask attached to a glass condenser to minimize evaporation. A magnetic stirrer equipped with a temperature controller (MTOPS; Ms300 Hs) was used to agitate the slurry at 400 rpm. Each experiment began with the mixing of 50 mL of sulfuric acid at a predetermined concentration with the required amount of $KMnO_4$. After bringing the solution to the required temperature, a 5-g black paste sample was added at a solid-to-liquid ratio of 1/10 (w/v). Following completion of the leaching experiment, the slurry was filtered through Whatman 1 filter paper, and the residues were washed with deionized water. Before washing, the pH of the pregnant leach solution (PLS) was measured using a pH meter (Hach, HQ40d) coupled with a pH probe (IntelliCAL PHC 28,101). The collected solutions were measured and analysed by AAS and ICP-MS. The dissolution percentages of the metals were calculated based on Eq. 1. To prevent ion interference during the AAS analyses, standard solutions and leachate dilutions were prepared in potassium chloride (KCl; Merck) at a concentration of 1 g/L. The chemicals were of analytical grade and used without any purification. Deionized water was used for dilutions.

$$\text{Dissolution}(\%) = \frac{C_t * V_F}{W_0 * H_0} \times 100 \qquad (1)$$

where C_t is the metal concentration in the leachate (mg/L), V_F is the volume of the analyzed leachate (L), H_0 is the metal concentration in the feeding (mg/kg), and W_0 is the weight of the feeding sample (kg).

Li-bearing liquors recovered from the oxidative leaching studies were subjected to impurity removal tests in the conditions determined to be optimum. A typical impurity removal experiment was conducted at 25 °C using 50 mL of the solution heated in a glass beaker using a temperature-controlled magnetic stirrer. Aluminium foil was used to cover the glass beaker during the experiment. The precipitating agent (NaOH; Merck) was added gradually with a syringe while stirring at a speed of 250 rpm once the solution reached the desired temperature. The addition of NaOH precipitated the solution in hydroxide form, increasing the pH of the solution, which was measured using a pH meter. After the

precipitation experiment, the slurry was filtered and the precipitate was rinsed in deionized water to remove any remaining contaminants. The collected solutions were measured and analyzed by AAS and ICP-MS. The precipitation percentage of the metal values was calculated based on Eq. 2.

$$\text{Precipitation}_{(M)}(\%) = \frac{[C_I * V_I - (C_F * V_F + C_W * V_W)]}{C_I * V_I} \times 100 \quad (2)$$

where M is the metal, C_I, C_F, and C_W are the test solution, filtrate, and wash liquor concentrations (mg/L) of the lithium, and V_I, V_F, and V_W are the test solution, filtrate, and wash liquor volume (L), respectively.

RESULTS AND DISCUSSION

Materials Characterization

The sample with a predetermined mass was completely dissolved in aqua regia (HCl:HNO_3 = 3:1, volume ratio) to reveal the basic metal composition through AAS and ICP-MS. Although the carbon content was not calculated, it was observed that the carbon material, which is characteristic of lithium-ion batteries, floated on the aqua regia solution for a while due to its hydrophobic nature. In particular, XRF analysis was also performed to determine the major Mn content. The basic metal contents of the lithium manganese dioxide black paste are shown in Table II.

The morphological properties of the material were investigated by SEM analysis. As can be seen from the micrograph in Fig. 2, the powder consists of homogeneous and dispersed amorphous particles, with sizes ranging from 0.5 to 22 μm with an average size of ≈ 7 μm. The particle sizes were revealed by WipFrag 4 image-based granulometry software using SEM micrographs. The morphological properties of the material are similar to the spent battery pastes in previous studies.[47–49]

The XRD spectrum of the material showed that the black paste mainly contained graphite (PDF card No.: 89-7213), lithium manganese oxide (PDF card No.: 44-0147), and lithium nickel oxide (PDF card No.: 85-1982) compounds (Fig. 3). The broadening peaks in the XRD spectrum indicate halo structures, which show that the material contains an amorphous phase.

Table II. The metal contents of the lithium manganese dioxide black paste

Element	Li	Mn	Ni	Co
wt.%	3.85	35.6	0.17	0.02

Leaching Experiments Without Oxidant

The dissolution of valuable metals from the $Li_{0.3}MnO_2$ and $Li_{0.55}Mn_{0.55}(NiO_2)$ materials during sulfuric acid leaching can be explained by the following reactions (Eqs. 3–9), indicating that these reactions occur spontaneously. The standard free energy ($\Delta G°_{298}$ = − 779 kJ/mol), enthalpy ($\Delta H°_{298}$= 834 kJ/mol), and entropy ($S°_{298}$ = 80 J/K mol) values of the $LiMnO_2$ at 25 °C were calculated based on density functional theory.[46] In order to maximize the dissolution of lithium while minimizing the leaching of manganese, nickel, and cobalt impurities, the suitable experimental conditions were selected to be a sulfuric acid concentration of 1.25 M, leaching time of 60 min, and leaching temperature of 60 °C (E4 conditions). The experimental results of the preliminary leaching tests are given in Table III.

$$\begin{aligned} &LiMnO_2(s) + 4H^+(aq) + e^- \\ &= Li^+(aq) + Mn^{2+}(aq) + 2H_2O(l) \\ &\Delta G°_{303} = -269.772\,\text{kJ} \end{aligned} \quad (3)$$

$$\begin{aligned} &2Li(s) + 2H_2O(l) = 2LiOH(s) + H_2(g) \\ &\Delta G°_{303} = -403.642\text{kJ} \end{aligned} \quad (4)$$

$$\begin{aligned} &LiOH(s) + H^+(aq) = Li^+(aq) + H_2O(l) \\ &\Delta G°_{303} = -91.325\text{kJ} \end{aligned} \quad (5)$$

$$\begin{aligned} &Li_2O(s) + 2H^+(aq) = 2Li^+(aq) + H_2O(l) \\ &\Delta G°_{303} = -260.529\text{kJ} \end{aligned} \quad (6)$$

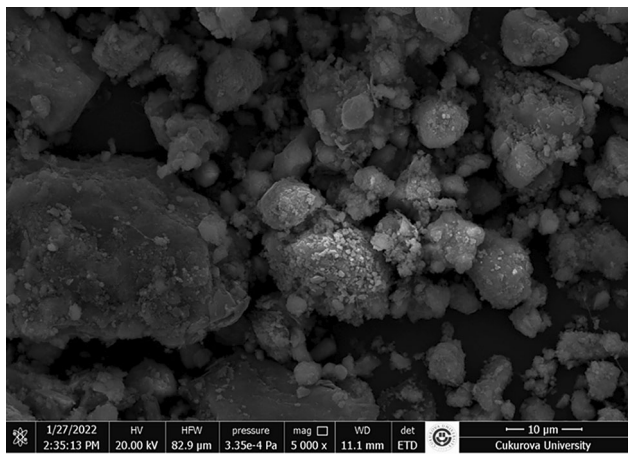

Fig. 2. SEM image of lithium manganese dioxide black paste.

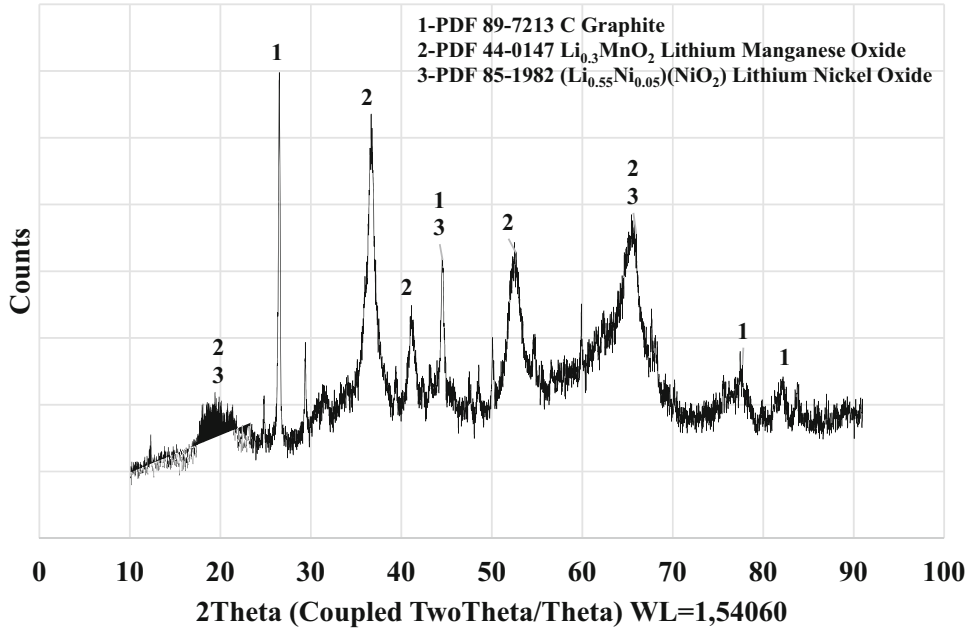

Fig. 3. XRD pattern of lithium manganese dioxide black paste.

Table III. Experimental results of preliminary leaching tests

Exp. No	Li dissolution (%)	Mn dissolution (%)	Ni dissolution (%)	Co dissolution (%)	pH (± 0.05)
E1	66.8	4.9	34.7	13.6	1.82
E2	76.8	9.8	44.2	15.1	1.73
E3	79.2	11.0	46.5	16.7	2.19
E4	93.0	13.3	46.6	19.5	0.69
E5	96.4	22.1	54.4	42.6	0.54
E6	90.9	8.8	45.3	13.3	0.47
E7	99.0	20.2	49.8	38.9	0.17
E8	86.6	7.7	43.9	14.5	0.16
E9	93.8	21.5	51.6	32.5	0.13

$$\mathrm{MnO_2}(s) + 4\mathrm{H^+}(aq) + 2e^- = \mathrm{Mn^{2+}}(aq) + \mathrm{H_2O}(l) \qquad \Delta G^\circ_{303} = -234.549\mathrm{kJ} \tag{7}$$

$$\mathrm{NiO}(s) + 2\mathrm{H^+}(aq) = \mathrm{Ni^{2+}}(aq) + \mathrm{H_2O}(l) \qquad \Delta G^\circ_{303} = -70.757\mathrm{kJ} \tag{8}$$

$$\mathrm{CoO}(s) + 2\mathrm{H^+}(aq) = \mathrm{Co^{2+}}(aq) + \mathrm{H_2O}(l) \qquad \Delta G^\circ_{303} = -76.945\,\mathrm{kJ} \tag{9}$$

Figure 4 shows the values obtained by converting the experimental results to the S/N ratio using the Taguchi approach. The S/N ratio values show that the most effective parameter for Li dissolution is determined as the H_2SO_4 concentration. Depending on the S/N ratio, the efficacy of the experimental parameters was ordered as follows: H_2SO_4 concentration > reaction temperature > reaction time. Considering the S/N ratios established for Mn, Ni, and Co dissolutions, the better results are obtained at the lowest parameter values, in accordance with the "smaller is better" approach.

These findings are in good agreement with the contribution ratio (C-Ratio) that indicates the ratio of effect of each parameter on the leaching performance of Li, Mn, Ni, and Co. The C-Ratio value was determined based on analysis of variance, which is inserted into the online supplementary material (see supplementary Table S1). The C-Ratio values for the Li dissolution were 80.12% and 17.37% for the acid concentration and time, respectively. The effect of temperature was negligible for the Li extraction (C-Ratio value: 0.54%). Similar results were determined for the Mn dissolution from the sample, for which the C-Ratio values of acid concentration and time were determined as 31.16% and 54.61%, respectively, while temperature had a minimum effect on the Mn extraction, with a C-Ratio value of 0.43%. Furthermore, acid

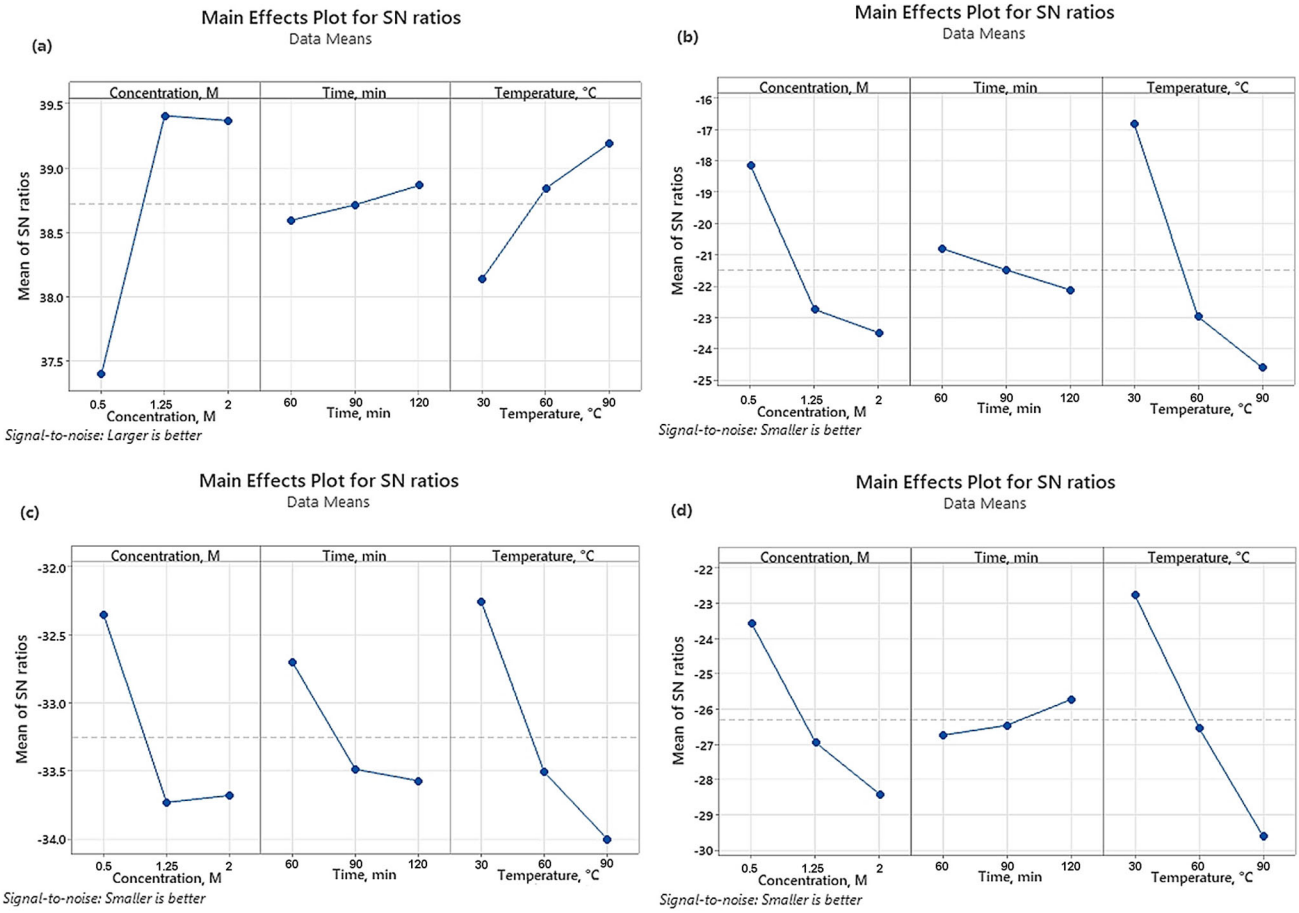

Fig. 4. S/N values for dissolution: (a) lithium (larger is better), (b) manganese (smaller is better), (c) nickel (smaller is better), and (d) cobalt (smaller is better).

concentration and time had strong effects on the Ni and Co extractions from the sample.

Leaching Experiment with Oxidant ($KMnO_4$)

At 60 °C and a solid–liquid ratio of 1/10, oxidative leaching experiments were conducted in 1.25 M sulfuric acid solutions in order to determine the influence of the quantity of $KMnO_4$ on the separation of lithium from manganese. The oxidant concentration ranged from 0.025 to 0.075 M. The experimental results are illustrated in Fig. 5, showing that the manganese and cobalt dissolutions were significantly decreased with increasing $KMnO_4$ concentration, while the lithium dissolution (84.8%) was slightly lower than when no oxidant was added (93%) (Table III, E4 conditions). In contrast, the rise in oxidant concentration kept the nickel dissolution constant (46.6%). In the present work, solution-phase oxidation is represented as the interaction of aqueous-phase manganese ions with the oxidant to form the manganese solid phase (Eq. 10). E° values for cobalt (III) to cobalt (II) are greater than E° values for permanganate anion to manganese (II). Therefore, permanganate ion can theoretically be utilized as an oxidant to separate manganese from cobalt (Eqs. 11 and 12). The manganese dissolution in the absence of oxidant was 13.3%. The decrease in dissolving was more dramatic with manganese, as demonstrated by the fact that 0.9% of manganese was dissolved in the presence of 0.075 $MKMnO_4$. During the leaching procedure, divalent manganese was oxidized into its trivalent or tetravalent species. The cobalt dissolution, on the other hand, was significantly decreased to 9.7% from 19.5% when the $KMnO_4$ concentration increased up to 0.075 M. This is a result of cobalt adsorption on fine MnO_2 particles or oxidation of divalent cobalt into its trivalent state. In the oxidative leaching experiments, the current researchers expected that the lithium dissolution percentages would remain constant, whereas manganese and cobalt concentrations gradually decreased. However, we observed that potassium permanganate has in particular a reverse effect on lithium dissolution at low concentration (0.025 M). This is due to the adsorption of lithium ions onto the bulk of the MnO_2 particles in the sample. The lithium dissolution is significantly decreased, 62.7% from 93%, and then slightly increased up to 84.8% at a 0.075-M $KMnO_4$ concentration. The optimal

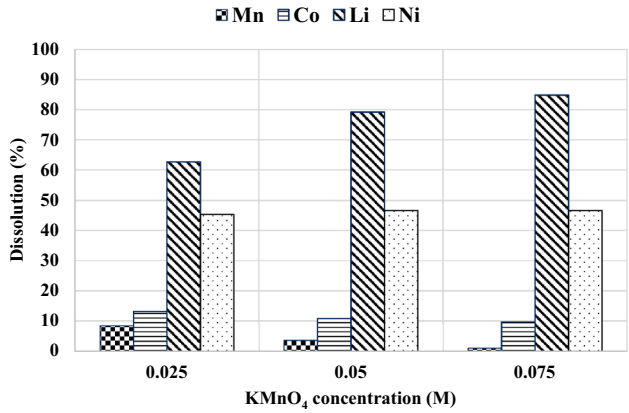

Fig. 5. Dissolution percentages of metals versus $KMnO_4$ concentration under the E4 conditions: acid concentration: 1.25 M, leaching time: 60 min, leaching temperature: 60 °C.

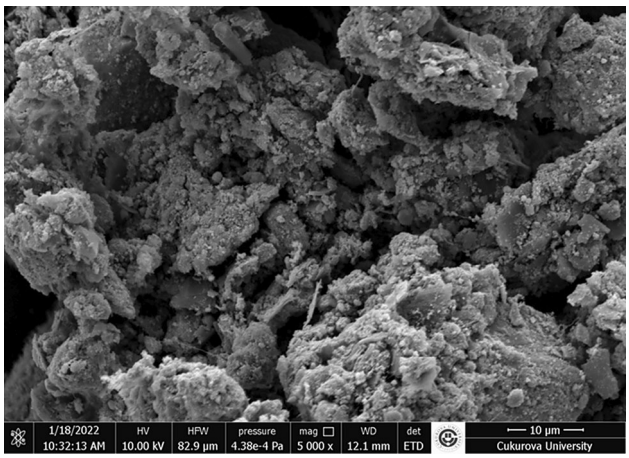

Fig. 6. SEM image of lithium manganese dioxide black paste after oxidative leaching under the optimum leaching conditions.

conditions for the selective leaching of lithium were determined to be 1.25 M sulfuric acid and 0.075 M $KMnO_4$ at 60 °C with a solid-to-liquid ratio of 1/10 and a leaching time of 60 min. Figure 6 shows the SEM images of lithium manganese dioxide black paste after the oxidative leaching experiment under the optimum conditions. Compared with the lithium manganese dioxide black paste in Fig. 2, the surface morphologies of the leached residue have plenty of pores of different sizes. Supplementary Table S2 shows the assay of the oxidative leaching results obtained under the optimum conditions.

$$1.5Mn^{2+}(aq) + MnO_4^-(aq) + H_2O(l) = 2.5MnO_2(s) + 2H^+(aq) \quad \Delta G^\circ_{303} = -141.638\text{kJ} \tag{10}$$

$$MnO_4^-(aq) + 8H^+(aq) + 5e^- \leftrightarrow Mn^{2+}(aq) + 4H_2O(l) \quad E^\circ = 1.51\,\text{V} \tag{11}$$

$$Co^{3+}(aq) + e^- \leftrightarrow Co^{2+}(aq) \quad E^\circ = 1.95\,\text{V}. \tag{12}$$

Impurity Removal from Li-Bearing Oxidative Leach Liquor

Before considering the lithium carbonate precipitation experiments, the impurity removal stage is essential to achieve a clean Li-bearing solution. The removal of impurities from the pregnant leach solutions collected from the oxidative leaching with potassium permanganate under the determined optimum conditions was carried out using 5 M NaOH at a temperature of 25 °C and pH of 10. The period of the precipitating agent addition was 15 min followed by 60 min of aging time at 250 rpm stirring speed. Supplementary Table S3 shows the assay of the impurity removal stage using sodium hydroxide, and, as can be seen, the manganese, nickel, and cobalt were completely removed from the leach solution at pH 10. A substantial amount of lithium losses was observed during the impurity removal tests, which is ascribed to the adsorption of Li^+ on the finest manganese particles. The precipitation reactions of the lithium, manganese, nickel,

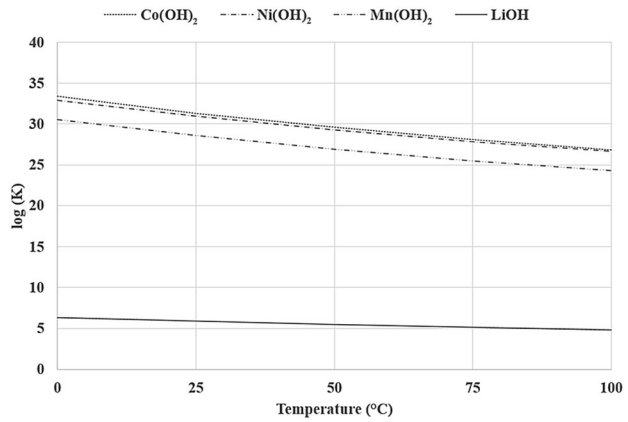

Fig. 7. Effect of temperature on equilibrium constants (HSC Chemistry 6.0 software).

and cobalt can be written according to Eqs. 13–16. Useful for the recovery of metal hydroxides, Fig. 7 depicts the equilibrium constants (log K) for the precipitation of lithium, manganese, nickel, and cobalt as a function of temperature over the range 0–100 °C. At 25 °C, the values of log K are seen to be in descending order: $Co(OH)_2$ $Ni(OH)_2 >$ $Mn(OH)_2 >$ LiOH. Figure 7 reveals that a high pH value requires precipitating Li^+ in a LiOH form due to the low value of log K.

$$Mn^{2+}(aq) + 2NaOH(aq) = Mn(OH)_2(s) + 2Na^+(aq) \quad \Delta G^\circ_{298} = -163.052\,kJ \tag{13}$$

$$Ni^{2+}(aq) + 2NaOH(aq) = Ni(OH)_2(s) + 2Na^+(aq) \quad \Delta G^\circ_{298} = -176.505\,kJ \tag{14}$$

$$Co^{2+}(aq) + 2NaOH(aq) = Co(OH)_2(s) + 2Na^+(aq) \quad \Delta G^\circ_{298} = -178.845\,kJ \tag{15}$$

$$Li^+(aq) + NaOH(aq) = LiOH(s) + Na^+(aq) \quad \Delta G^\circ_{298} = -33.649\,kJ \tag{16}$$

After the impurity removal stage, the collected solution can be fed to the lithium carbonate precipitation section, which will be presented at a high temperature in further studies of this research group. The sodium carbonate addition is calculated as the times of stoichiometric sodium carbonate requirement for the total molar concentration of lithium ion in the PLS to precipitate as carbonate. In order to accelerate the precipitation of lithium, a seed addition can be considered in the Li-bearing leach solution. The precipitation reactions of the lithium are written according to Eqs. 17 and 18.

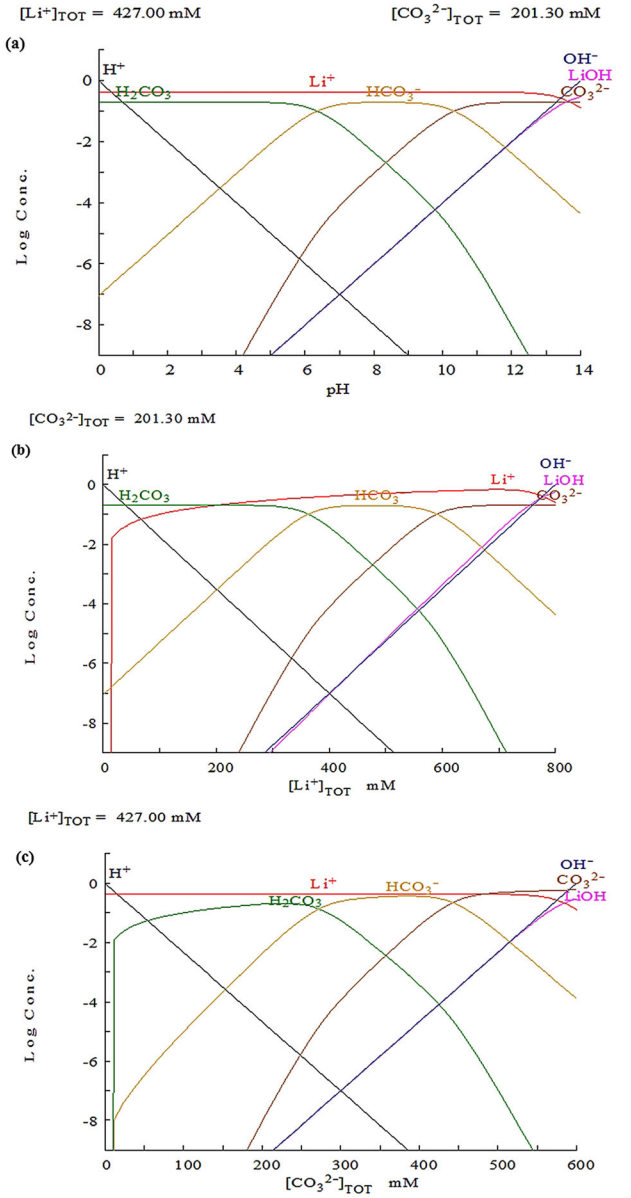

Fig. 8. Speciation diagrams: (a) Li as a function of pH using 427 mM of lithium and 201.3 mM of carbonate; (b) Li as a function of Li^+ concentration using an excess amount of carbonate; and (c) Li as a function of carbonate using 427 mM of lithium (MEDUSA/HYDRA Software).

$$Na_2CO_3(s) = 2Na^+(aq) + CO_3^{2-}(aq) \quad \Delta G^\circ_{298} = -3.610\,kJ \tag{17}$$

$$2Li^+(aq) + CO_3^{2-}(aq) = Li_2CO_3(s) \quad \Delta G^\circ_{363} = -27.486\,kJ \tag{18}$$

To determine the thermodynamic viability of various aqueous species, the species of lithium as a function of pH, lithium concentration, and carbonate concentration was assessed at standard temperature and pressure using Medusa-Hydra software. Lithium species can exist in the pH range

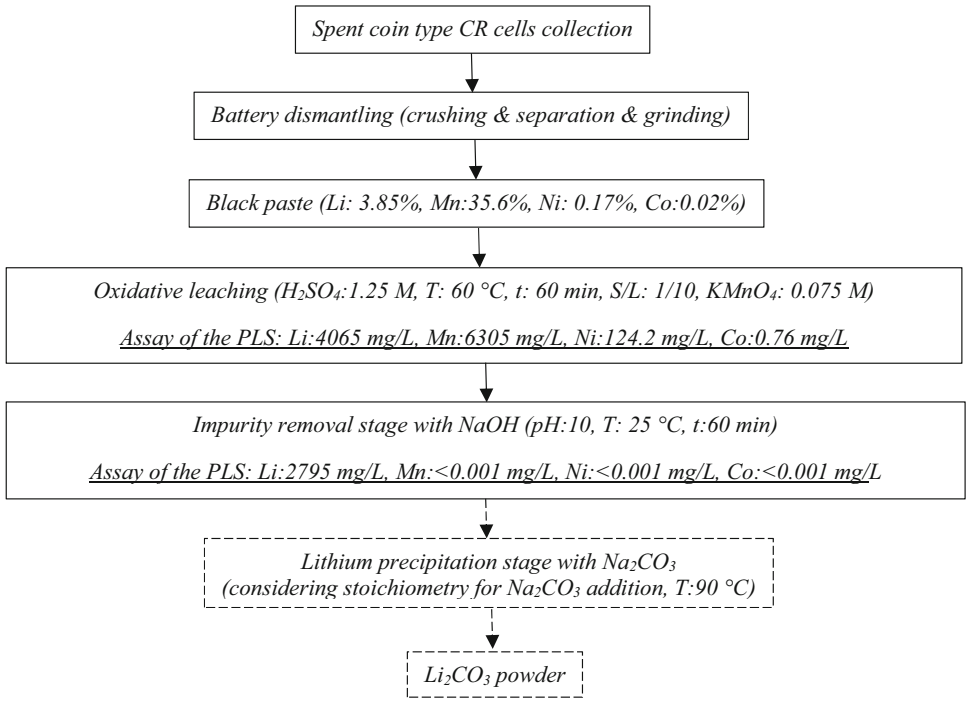

Fig. 9. Proposed possible flow chart for Li_2CO_3 production from spent coin-type CR cells; *dashed line* further studies on the oxidative leach solution.

0–14 when lithium and carbonate concentrations are 427 mM and 201.3 mM, respectively, as depicted in Fig. 8a. Because of the concentration of PLS in the leachate and the stoichiometric ratio, the lithium and carbonate concentrations are calculated to be 427 mM and 201.3 mM, respectively. Figure 8b illustrates the speciation behavior of lithium as a function of Li^+ concentration when using an excess amount of carbonate and a pH range of 0–14. Figure 8c indicates the speciation behavior of lithium as a function of Li^+ concentration, when an excess amount of carbonate is used with respect to 427 mM lithium in entire ranges of the pH. As the pH increases to 14, the concentrations of H_2CO_3 and HCO_3^- drop, and the potential for lithium precipitation in the form of lithium carbonate reaches its maximum. Therefore, the precipitation of lithium as lithium carbonate is thermodynamically feasible according to the MEDUSA/HYDRA and HSC Chemistry software results. A possible flowsheet for the production of Li_2CO_3 from spent coin-type CR cells is demonstrated in Fig. 9. The selective leaching of lithium from the spent cells, leaving a bulky amount of manganese in the residue, was excellently achieved by oxidative leaching. The produced PLS at optimum conditions was subjected to an impurity removal stage with sodium hydroxide. It was determined that the selective precipitation in this stage has not been observed, as a substantial amount of lithium is precipitated along with manganese, nickel, and cobalt. In the last stage, the lithium precipitation as a form of Li_2CO_3 was evaluated by the MEDUSA/HYDRA and HSC Chemistry software, and it was found that the precipitation of Li_2CO_3 is thermodynamically feasible at high pH values. Based on these experimental results, a possible flow chart is proposed for this study.

CONCLUSION

Lithium recovery from lithium manganese dioxide black paste dismantled from spent coin-type CR cells has been investigated. In accordance with the Taguchi approach, dissolution values were interpreted according to the S/N ratios, in which the philosophy was “larger is better” for Li dissolution and “smaller is better” for the other element extractions. As a result of oxidant-free leaching with sulfuric acid, 93% of the lithium was taken into the leach solution, along with 13.3% Mn, 46.6% Ni, and 19.5% Co under optimum conditions: sulfuric acid concentration of 1.25 M, leaching time of 60 min, and leaching temperature of 60 °C. Notably, the Mn dissolution value decreased to 0.9% from 13.3% with the addition of 0.075 M $KMnO_4$ oxidant. After oxidative leaching, the manganese, nickel, and cobalt were completely removed from the leach solution at pH 10. The final Li-bearing liquor was determined to be 2795 mg/L Li content. For Li_2CO_3 production, the speciation of lithium as a function of pH, lithium concentration, and carbonate concentration was evaluated at standard temperature and pressure, using Medusa-Hydra software. The results proved that the precipitation of lithium as lithium carbonate is thermodynamically feasible. In the light of these experimental and theoretical

findings, a possible flow chart has been proposed. Homogeneous and heterogeneous reactive crystallization techniques will be applied to the pure Li_2SO_4 solution to produce Li_2CO_3 in future studies.

ACKNOWLEDGEMENTS

The authors thank Ismail Turkes from Ankara for supplying the spent coin-type lithium manganese dioxide CR cells.

CONFLICT OF INTEREST

On behalf of all authors, the corresponding author states that there is no conflict of interest.

SUPPLEMENTARY INFORMATION

The online version contains supplementary material available at https://doi.org/10.1007/s11837-022-05507-6.

REFERENCES

1. C. Peng, F. Liua, Z. Wang, B.P. Wilson, and M. Lundstrom, *J. Power Sources*. https://doi.org/10.1016/j.jpowsour.2019.01.072 (2019).
2. M. Contestabile, S. Panero, and B. Scrosati, *J. Power Sources*. https://doi.org/10.1016/S0378-7753(99)00261-X (1999).
3. T. Dolker and D. Pant, *Curr. Dev. Biotechnol. Bioeng.* https://doi.org/10.1016/B978-0-444-64321-6.00017-3 (2020).
4. J. Kondas, J. Jandov, and M. Nemeckova, *Hydrometallurgy*. https://doi.org/10.1016/j.hydromet.2006.05.009 (2006).
5. G. Granata, F. Pagnanelli, E. Moscardini, Z. Takacova, T. Havlik, and L. Toro, *J. Power Sources*. https://doi.org/10.1016/j.jpowsour.2012.04.016 (2012).
6. P. Meshram, B.D. Pandey, and T.R. Mankhand, *Hydrometallurgy*. https://doi.org/10.1016/j.hydromet.2014.10.012 (2014).
7. G. Martin, L. Rentsch, M. Hock, and M. Bertau, *Energy Storage Materials*. https://doi.org/10.1016/j.ensm.2016.11.004 (2017).
8. S. Castillo, F. Ansart, C. Laberty-Robert, and J. Portal, *J. Power Sources*. https://doi.org/10.1016/S0378-7753(02)00361-0 (2002).
9. "Lithium battery", https://en.wikipedia.org/wiki/Lithium_battery. Accessed 10 January 2021.
10. M.B.J.G. Freitas, V.C. Pegoretti, and M.K. Pietre, *J. Power Sources*. https://doi.org/10.1016/j.jpowsour.2006.10.050 (2007).
11. E. Van Eygen, S. De Meester, H.P. Tran, and J. Dewulf, *Resour. Conserv. Recycl.* https://doi.org/10.1016/j.resconrec.2015.10.032 (2016).
12. N.J. Boxall, S. King, K.Y. Cheng, Y. Gumulya, W. Bruckard, and A.H. Kaksonen, *Miner. Eng.* https://doi.org/10.1016/j.mineng.2018.08.030 (2018).
13. W.S. Chen, C.T. Liao, and K.Y. Lin, *Energy Proc.* https://doi.org/10.1016/j.egypro.2016.12.162 (2017).
14. H. Mekhalfi, N. Chelali, S. Benhamimid, O.M. Laib, B. Nessark, and A. Bahloul, *Russ. J. Appl. Chem.* https://doi.org/10.1134/S1070427215050249 (2015).
15. D. Hariprasad, B. Dash, M.K. Ghosh, and S. Anand, *Miner. Eng.* https://doi.org/10.1016/j.mineng.2007.07.013 (2007).
16. K.S. Abdel Halim, M. Bahgat, M.B. Morsi, and K. El-Barawy, *Ironmaking Steelmaking*. https://doi.org/10.1179/030192310X12827375731465 (2011).
17. M.K. Sinha, W. Purcell, and W.A. Van Der Westhuizen, *Miner. Eng.* https://doi.org/10.1016/j.mineng.2020.106406 (2020).
18. S. Xiong, X. Li, P. Liu, S. Hao, F. Hao, Z. Yin, and J. Liu, *Miner. Eng.* https://doi.org/10.1016/j.mineng.2018.06.003 (2018).
19. F. Wu, J. Deng, J. Kuang, Z. Xiao, H. Liu, M. Liang, P. Yu, and B. Mi, *Can. Metall. Q.* https://doi.org/10.1080/00084433.2020.1715692 (2020).
20. N. Peng, Q. Pan, H. Liu, Z. Yang, and G. Wang, *Miner. Eng.* https://doi.org/10.1016/j.mineng.2018.07.002 (2018).
21. P.K. Das, S. Anand, and R.P. Das, *Hydrometallurgy*. https://doi.org/10.1016/S0304-386X(98)00044-9 (1998).
22. C. Abbruzzese, M.Y. Duarte, B. Paponetti, and L. Toro, *Miner. Eng.* https://doi.org/10.1016/0892-6875(90)90126-V (1990).
23. X. Zhang, Z. Liu, X. Wu, J. Du, and C. Tao, *J. Electroanal. Chem.* https://doi.org/10.1016/j.jelechem.2017.02.009 (2017).
24. B. Liu, Y. Zhang, M. Lu, Z. Su, G. Li, and T. Jiang, *Miner. Eng.* https://doi.org/10.1016/j.mineng.2018.11.016 (2019).
25. S. Yuan, W. Zhou, Y. Han, and Y. Li, *Miner. Eng.* https://doi.org/10.1016/j.mineng.2020.106359 (2020).
26. M.K. Sinha and W. Purcell, *Hydrometallurgy*. https://doi.org/10.1016/j.hydromet.2019.05.021 (2019).
27. R.A. Amiliana, P.T. Wulandari, I.T. Ramadhan, and F.A. Kusumadewi, *Mater. Sci. Eng.* https://doi.org/10.1088/1757-899X/333/1/012041 (2018).
28. X.L. Zeng, J.H. Li, and B.Y. Shen, *J. Hazard. Mater.* https://doi.org/10.1016/j.jhazmat.2015.02.064 (2015).
29. P. Meshram, B.D. Abhilash, and T.R. Pandey, *J. Ind. Eng. Chem.* https://doi.org/10.1016/j.jiec.2016.07.056 (2016).
30. X.P. Chen, L. Cao, D.Z. Kang, J.Z. Li, T. Zhou, and H.R. Ma, *Waste Manage.* https://doi.org/10.1016/j.wasman.2018.09.013 (2018).
31. R.C. Wang, Y.C. Lin, and S.H. Wu, *Hydrometallurgy*. https://doi.org/10.1016/j.hydromet.2009.08.005 (2009).
32. L. Sun and K.Q. Qiu, *Waste Manage.* https://doi.org/10.1016/j.wasman.2012.03.027 (2012).
33. Y.F. Huang, G.H. Han, J.T. Liu, W.C. Chai, W.J. Wang, S.Z. Yang, and S.P. Su, *J. Power Sources*. https://doi.org/10.1016/j.jpowsour.2016.06.072 (2016).
34. Q. Li, K.Y. Fung, K.M. Ng, and A.C.S. Sustain, *Chem. Eng.* https://doi.org/10.1021/acssuschemeng.9b00590 (2019).
35. Y. Pranolo, W. Zhang, and C.Y. Cheng, *Hydrometallurgy*. https://doi.org/10.1016/j.hydromet.2010.01.007 (2010).
36. R. Sattar, S. Ilyas, H.N. Bhatti, and A. Ghaffar, *Sep. Purif. Technol.* https://doi.org/10.1016/j.seppur.2018.09.019 (2019).
37. J. Kang, G. Senanayake, J. Sohn, and S.M. Shin, *Hydrometallurgy*. https://doi.org/10.1016/j.hydromet.2009.10.010 (2010).
38. X. Zeng, J. Li, and B. Shen, *J. Hazard Mater.* https://doi.org/10.1016/j.jhazmat.2015.02.064 (2015).
39. X. Chen, D. Kang, L. Cao, J. Li, T. Zhou, and H. Ma, *Sep. Purif. Technol.* https://doi.org/10.1016/j.seppur.2018.08.072 (2019).
40. Y. Yang, S.M. Xu, and Y.H. He, *Waste Manage.* https://doi.org/10.1016/j.wasman.2017.03.018 (2017).
41. S.Y. Lei, Y. Cao, X.F. Cao, W. Sun, Y.Q. Weng, and Y. Yang, *Sep. Purif. Technol.* https://doi.org/10.1016/j.seppur.2020.117258 (2020).
42. T. Liu, J. Chen, H. Li, and K. Li, *Sep. Purif. Technol.* https://doi.org/10.1016/j.seppur.2020.116869 (2020).
43. T. Liu, J. Chen, H. Li, K. Li, and D. Li, *Hydrometallurgy*. https://doi.org/10.1016/j.hydromet.2019.06.008 (2019).
44. L. Chen, H. Li, J. Chen, D. Li, and T. Liu, *Miner. Eng.* https://doi.org/10.1016/j.mineng.2020.106232 (2020).
45. D. Wang, X. Zhang, H. Chen, and J. Sun, *Miner. Eng.* https://doi.org/10.1016/j.mineng.2018.06.023 (2018).
46. M. Tuccillo, O. Palumbo, M. Pavone, A.B. Munoz-Garcia, A. Paolone, and S. Brutti, *Curr. Comput.-Aided Drug Des.* https://doi.org/10.3390/cryst10060526 (2020).
47. J. Guan, Y. Li, Y. Guo, R. Su, G. Gao, H. Song, H. Yuan, B. Liang, and Z. Guo, *ACS Sustainable Chem. Eng.* https://doi.org/10.1021/acssuschemeng.6b02337 (2017).

48. B.J. Forero, J.V. Díaz-Salaverría, P. Delvasto and C.X. Gouveia, *WASTES – Solutions, Treatments and Opportunities II*, Ed. C. Vilarinho, F. Castro and M.D.L. Lopes (CRC press, London, 2017) https://doi.org/10.1201/9781315206172.
49. M. Rashid and A. Gupta, *Electrochim. Acta*. https://doi.org/10.1016/j.electacta.2017.02.040 (2017).